

## Supplementary information

### Chemically oxidized $\gamma$ -MnO<sub>2</sub> for lithium secondary batteries; structure and intercalation / deintercalation properties†

Won Il Jung,<sup>a</sup> Miki Nagao,<sup>a</sup> Cédric Pitteloud,<sup>a</sup> Keiji Itoh,<sup>b</sup> Atsuo Yamada,<sup>a</sup> and Ryoji Kanno<sup>\*,a</sup>

<sup>a</sup> Department of Electronic Chemistry, Interdisciplinary Graduate School of Science and Engineering, Tokyo Institute of Technology, 4259 Nagatsuta, Midori-ku, Yokohama 226-8502, Japan

<sup>b</sup> Research Reactor Institute, Kyoto University, Kumatori-cho, Sennan-gun 590-0494, Japan

E-mail: wjung@echem.titech.ac.jp

\*corresponding author: Tel.: 81-45-924-5401, Fax: 81-45-924 5409

E-mail: kanno@echem.titech.ac.jp (R. Kanno)

**Background of the structure for  $\gamma$ -MnO<sub>2</sub>; the existence of cation vacancies and protons and the oxidation mechanism of  $\gamma$ -MnO<sub>2</sub>.**

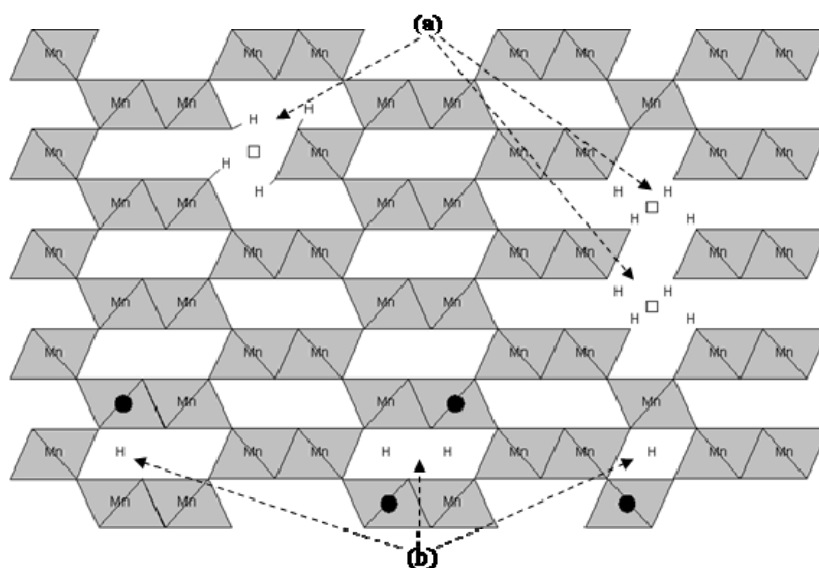
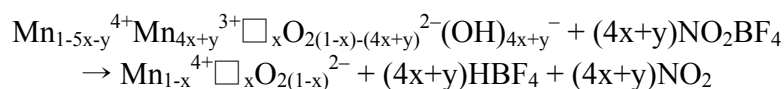


**Fig. S1** Schematic drawing of the model structure for  $\gamma$ -MnO<sub>2</sub> and the position of the protons; (a) position of the Ruetschi protons, and (b) position of the Coleman protons. □ and ● denote cation vacancy and Mn<sup>3+</sup> defect, respectively.

One of the structural characteristic of  $\gamma$ -MnO<sub>2</sub> is the existence of cation vacancies and protons in the structure. Ruetschi proposed that there are vacancies in the Mn<sup>4+</sup> sublattice in the MnO<sub>2</sub> and each empty Mn<sup>4+</sup> site is coordinated to four protons in the form of OH<sup>-</sup> ions to compensate the charge of the manganese ions. These types of protons are called “Ruetschi” protons that are thought to be localized in the vacancy octahedron and be permanently occupied. Protons located in conjunction with Mn<sup>3+</sup> ions in the structure are called “Coleman” protons. Therefore, the chemical composition of  $\gamma$ -MnO<sub>2</sub> could be explained by this formulation: Mn<sub>1-5x-y</sub><sup>4+</sup>Mn<sub>4x+y</sub><sup>3+</sup>□<sub>x</sub>O<sub>2(1-x)-(4x+y)</sub><sup>2-</sup>(OH)<sub>4x+y</sub><sup>-</sup>, where □ denotes cation vacancy.

On the other hand, an oxidant, NO<sub>2</sub>BF<sub>4</sub> was used to remove the protons. The redox potential of NO<sub>2</sub><sup>+</sup>/NO<sub>2</sub> is about 5.1 V vs. Li/Li<sup>+</sup> and is effective in oxidizing  $\gamma$ -MnO<sub>2</sub>. Considering the oxidation mechanism of  $\gamma$ -MnO<sub>2</sub>, the oxidation reaction of  $\gamma$ -MnO<sub>2</sub> using NO<sub>2</sub>BF<sub>4</sub> could be described as below.



### Cycling data for chemically oxidized $\gamma\text{-MnO}_2$

Fig. S2 shows electrochemical cycling behavior for chemically oxidized  $\gamma\text{-MnO}_2$ . The cell showed a first discharge capacity of about 275 mAh/g, and a reversible capacity of about 250 mAh/g, which is the highest capacity among the  $\gamma\text{-MnO}_2$  prepared previously.

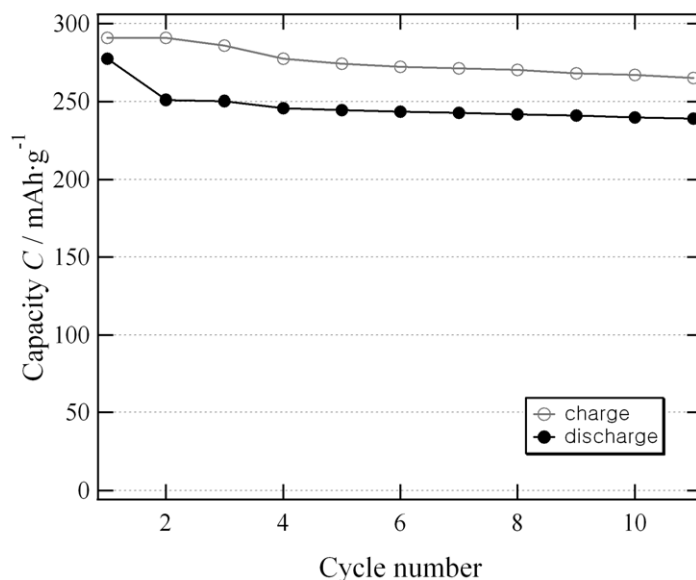
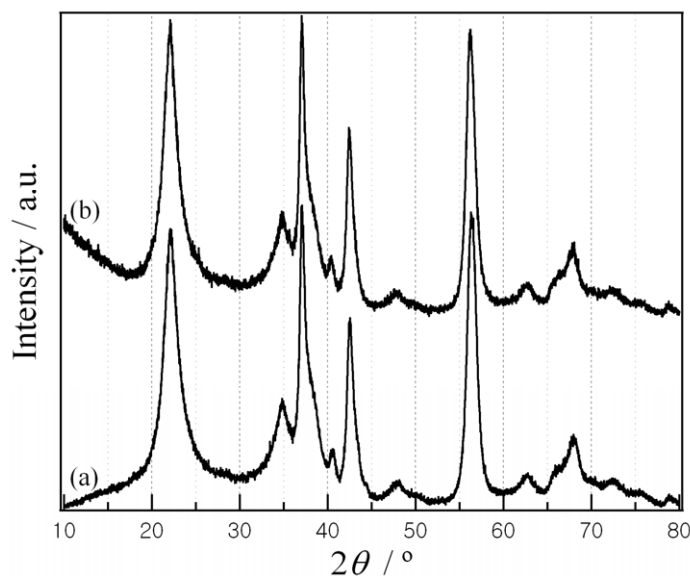


Fig. S2 Cycling data for chemically oxidized  $\gamma\text{-MnO}_2$ .

### Comparison of XRD patterns between before and after the chemical oxidation

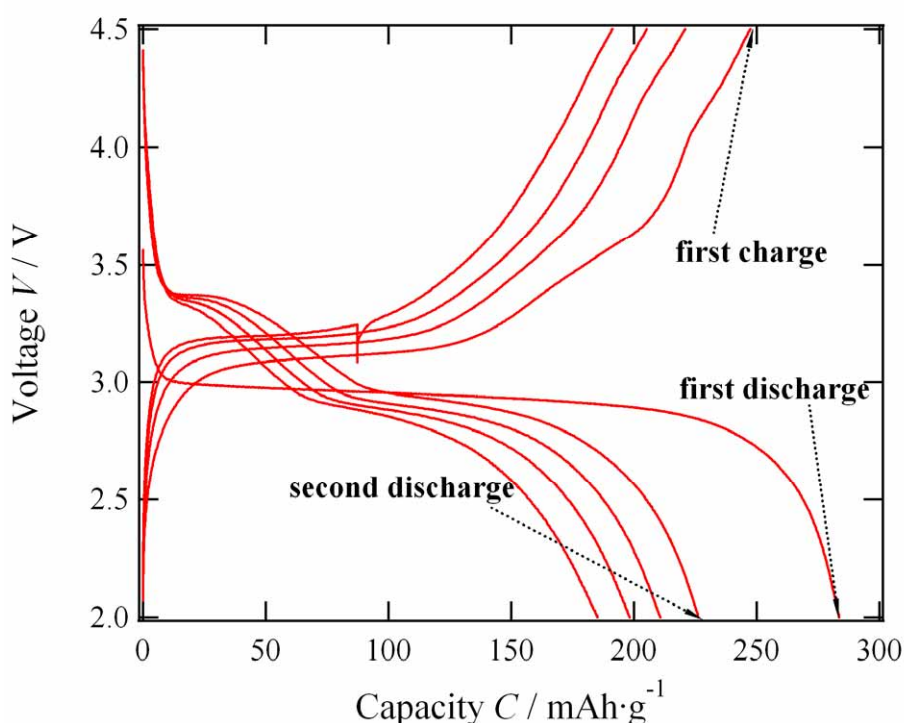
Fig. S3 shows the X-ray powder diffraction diagrams for untreated  $\gamma\text{-MnO}_2$  and chemically oxidized  $\gamma\text{-MnO}_2$  at optimized condition. These patterns are similar to those of conventional electrolytic manganese dioxides. No significant structural changes were observed during chemical oxidation process, and it could be thought that protons were removed without any changes in the structure of  $\gamma\text{-MnO}_2$  by the chemical oxidation process.



**Fig. S3** X-ray powder diffraction diagrams for  $\gamma$ -MnO<sub>2</sub>; (a) untreated  $\gamma$ -MnO<sub>2</sub> and (b) chemically oxidized  $\gamma$ -MnO<sub>2</sub>.

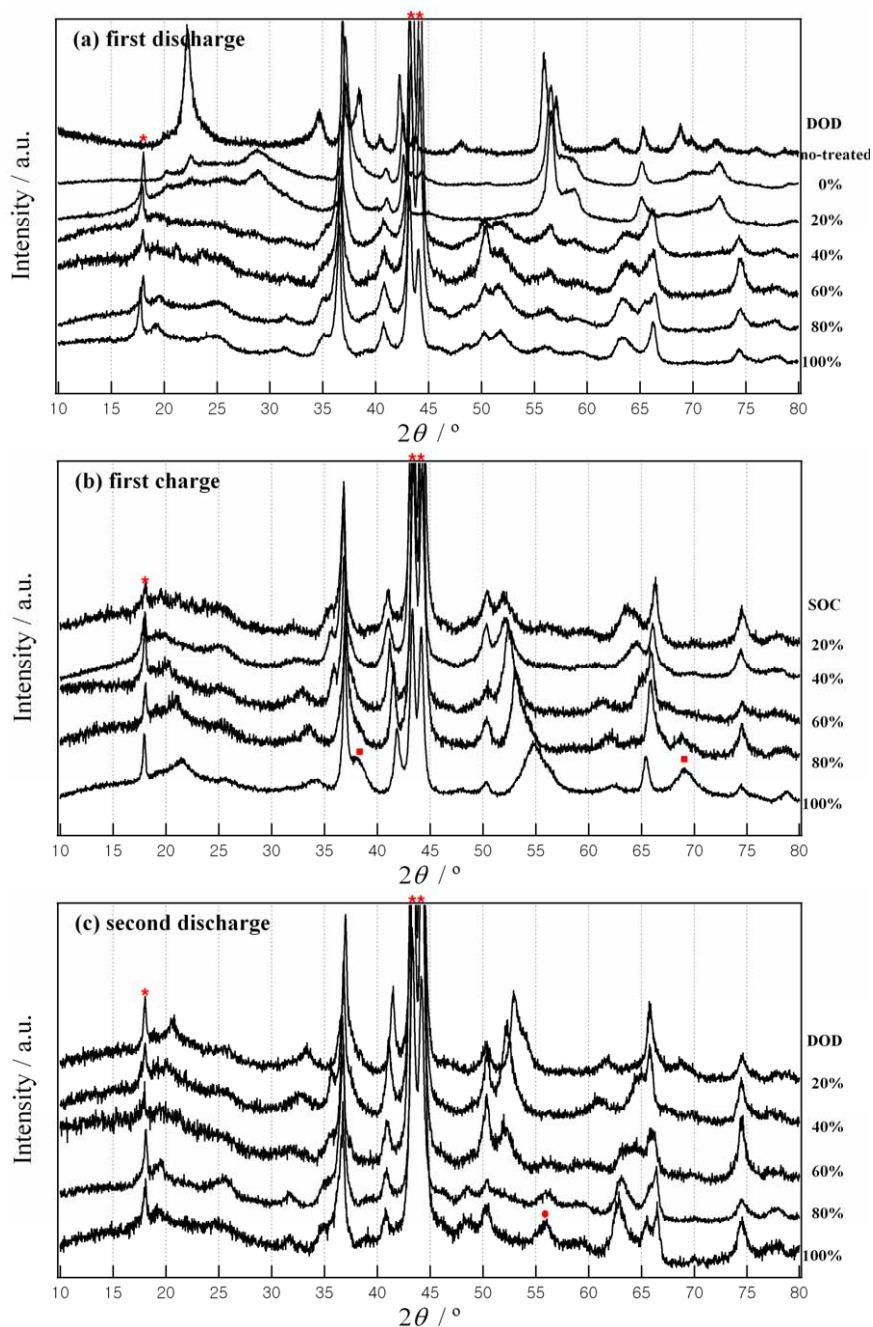
### Comparison of ex-situ XRD patterns during the first two cycles

For comparative purpose, the electrochemical performance of another  $\gamma$ -MnO<sub>2</sub> (product name RAM) was also examined under the same conditions as shown in Fig. S4. It should be noted that the first discharge capacity was calculated at 280 mAh/g, however, the capacity abruptly dropped to 185 mAh/g at the fifth discharge cycle. According to the first discharge curve, it has only one plateau around 3.0 V, which implies that this different electrochemical behavior could be caused by the collapse of Mn<sup>4+</sup> vacancy containing “Ruetschi” protons as reported in our previous work,<sup>20</sup> because structural changes could make reduction of possible lithium-inserting sites, resulting in a poor cyclability.



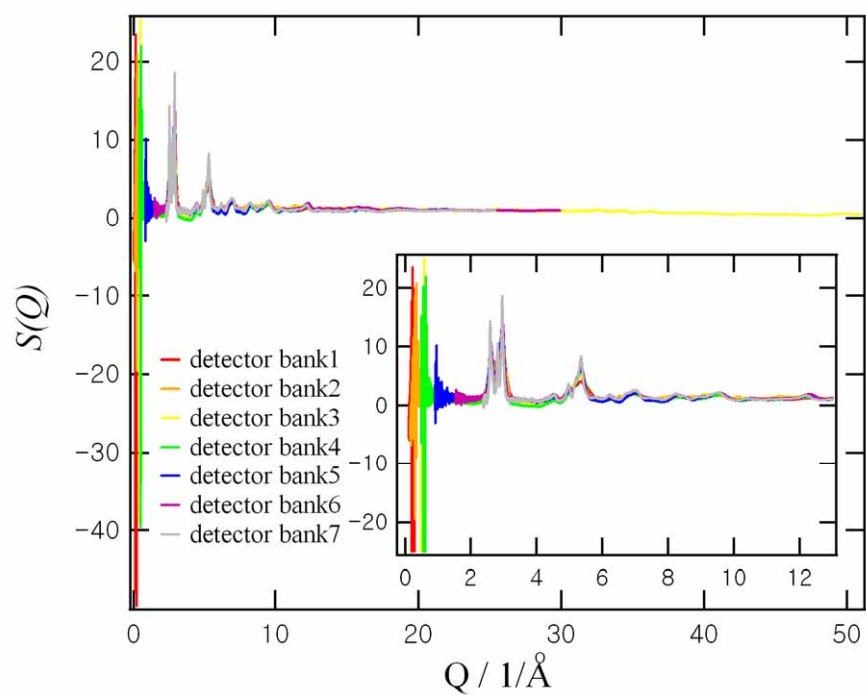
**Fig. S4** Charge-discharge profiles of chemically oxidized  $\gamma$ -MnO<sub>2</sub>(RAM) at optimized conditions.

Fig. S5 shows X-ray diffraction patterns of  $\gamma$ -MnO<sub>2</sub> (RAM) at different partial charge/discharge states. The diffraction patterns of chemically oxidized RAM were quite different with untreated RAM sample. The intensity of (110) peak ( $2\theta \cong 22^\circ$ ) decreased and a new peak appeared around  $29^\circ$  during the first discharge as illustrated in Figure S5(a). These phenomena are related to the phase transformation of  $\gamma$ -MnO<sub>2</sub> (RAM) from ramsdellite to pyrolusite. Moreover, new peaks are observed around  $38^\circ$  and  $69^\circ$  (marked in red squares) during the first charge in Figure S5(b) and around  $56^\circ$  (marked in red circle) during the second discharge in Figure S5(c), which could be caused by partial transformation from pyrolusite to ramsdellite. This partial transformation of  $\gamma$ -MnO<sub>2</sub> (RAM) is irreversible during the charge-discharge process, which might be a major reason for the poor cycling as shown in Figure S4.



**Fig. S5** Ex-situ X-ray diffraction patterns for  $\gamma$ - $\text{MnO}_2$  (RAM) at different partial charging/discharging states; (a) the first discharging state, (b) the first charging state and (c) the second discharging state (peaks marked with asterisk are due to sample holder).

**The information of data calculation for neutron total scattering**



**Fig. S6** The partial structure factors,  $S(Q)$  detected from each bank for chemically oxidized  $\gamma$ - $\text{MnO}_2$ .

**The data file format of DIFFaX simulation for  $\gamma$ -MnO<sub>2</sub> in Backus-Naur form**

{data file for ramsdellite}

INSTRUMENTAL {Header for instrumental section}  
X-RAY {Simulate X-ray diffraction}  
1.54050 {X-ray wavelength}  
{gaussian 0.1 trim} {Instrumental broadening (much faster)}  
PSEUDO-VOIGT 0.45 2.0 1.6 0.6 TRIM {Instrumental broadening (much slower)}

STRUCTURAL {Header for structural section}  
4.452 9.580 2.789 90.0 {unit cell coordinates, a, b, c, gamma}  
MMM {hexagonal, c = cubic [111]}  
4 {111 sheet, plus its mirror}

LAYER 1

NONE

Mn4+ 1 .5220 .3640 .7500 1.0 1.0  
Mn4+ 2 .4780 .6360 1.2500 1.0 1.0  
Mn4+ 3 .9780 .8640 1.7500 1.0 1.0  
Mn4+ 4 1.0220 1.1360 2.2500 1.0 1.0  
O 2- 1 .8330 .2250 .7500 1.0 0.3333  
O 2- 2 .3330 .2750 .2500 1.0 0.3333  
O 2- 3 .7110 .4670 .2500 1.0 0.5  
O 2- 4 .2890 .5330 1.7500 1.0 0.5  
O 2- 5 .3330 .2750 1.2500 1.0 0.3333  
O 2- 6 .7110 .4670 1.2500 1.0 0.5  
O 2- 7 .2890 .5330 .7500 1.0 0.5  
O 2- 8 .6670 .7250 .7500 1.0 0.3333  
O 2- 9 .1670 .7750 1.2500 1.0 0.3333  
O 2- 10 .6670 .7250 1.7500 1.0 0.6667  
O 2- 11 .7890 .9670 1.2500 1.0 0.5  
O 2- 12 1.2110 1.0330 1.7500 1.0 0.5  
O 2- 13 .8330 1.2250 1.7500 1.0 0.3333  
O 2- 14 1.3330 1.2750 2.2500 1.0 0.3333  
O 2- 15 .8330 1.2250 2.7500 1.0 0.3333  
O 2- 16 1.2110 1.0330 2.7500 1.0 0.5  
O 2- 17 .7890 .9670 2.2500 1.0 0.5  
O 2- 18 1.1670 .7750 2.2500 1.0 0.3333  
O 2- 19 1.1670 .7750 1.2500 1.0 0.3333

LAYER 2

NONE

Mn4+ 1 .5830 .3640 .7500 1.0 1.0  
Mn4+ 2 .5000 .6360 1.2500 1.0 1.0

Mn4+	3	.9170	.8640	1.7500	1.0	1.0
Mn4+	4	1.0000	1.1360	2.2500	1.0	1.0
O 2-	1	.8330	.2250	.7500	1.0	0.3333
O 2-	2	.4550	.2750	.2500	1.0	0.3333
O 2-	3	.8330	.4670	.2500	1.0	0.5
O 2-	4	.2890	.5330	1.7500	1.0	0.5
O 2-	5	.3330	.2750	1.2500	1.0	0.3333
O 2-	6	.7110	.4670	1.2500	1.0	0.5
O 2-	7	.3330	.5330	.7500	1.0	0.5
O 2-	8	.7110	.7250	.7500	1.0	0.3333
O 2-	9	.2890	.7750	1.2500	1.0	0.3333
O 2-	10	.6670	.7250	1.7500	1.0	0.6667
O 2-	11	.6670	.9670	1.2500	1.0	0.5
O 2-	12	1.1670	1.0330	1.7500	1.0	0.5
O 2-	13	.7890	1.2250	1.7500	1.0	0.3333
O 2-	14	1.2110	1.2750	2.2500	1.0	0.3333
O 2-	15	.8330	1.2250	2.7500	1.0	0.3333
O 2-	16	1.2110	1.0330	2.7500	1.0	0.5
O 2-	17	.7890	.9670	2.2500	1.0	0.5
O 2-	18	1.1670	.7750	2.2500	1.0	0.3333
O 2-	19	1.0450	.7750	1.2500	1.0	0.3333

### LAYER 3

NONE

Mn4+	1	.5220	.3640	.7500	1.0	1.0
Mn4+	2	1.0220	.6360	1.2500	1.0	1.0
Mn4+	3	.5220	.8640	1.7500	1.0	1.0
Mn4+	4	1.0220	1.1360	2.2500	1.0	1.0
O 2-	1	.8330	.2250	.7500	1.0	0.3333
O 2-	2	.3330	.2750	.2500	1.0	0.3333
O 2-	3	.7110	.4670	.2500	1.0	0.3333
O 2-	4	1.2110	.5330	1.7500	1.0	0.3333
O 2-	5	.3330	.2750	1.2500	1.0	0.3333
O 2-	6	.7110	.4670	1.2500	1.0	0.6667
O 2-	7	.2890	.5330	.7500	1.0	0.3333
O 2-	8	.8330	.7250	.7500	1.0	0.3333
O 2-	9	1.2550	.7750	1.2500	1.0	0.3333
O 2-	10	.8330	.7250	1.7500	1.0	0.6667
O 2-	11	.7110	.9670	1.2500	1.0	0.3333
O 2-	12	.2890	1.0330	1.7500	1.0	0.3333
O 2-	13	.8330	1.2250	1.7500	1.0	0.3333
O 2-	14	1.2550	1.2750	2.2500	1.0	0.3333
O 2-	15	.8330	1.2250	2.7500	1.0	0.3333

O 2- 16 1.2110 1.0330 2.7500 1.0 0.3333  
O 2- 17 .7110 .9670 2.2500 1.0 0.6667  
O 2- 18 .3330 .7750 2.2500 1.0 0.3333  
O 2- 19 .3330 .7750 1.2500 1.0 0.3333  
O 2- 20 1.2110 .5330 .7500 1.0 0.3333  
O 2- 21 1.2110 1.0330 1.7500 1.0 0.3333

#### LAYER 4

NONE

Mn4+ 1 .5220 .3640 .7500 1.0 1.0  
Mn4+ 2 1.0220 .6360 1.2500 1.0 1.0  
Mn4+ 3 .5220 .8640 1.7500 1.0 1.0  
Mn4+ 4 1.0220 1.1360 2.2500 1.0 1.0  
O 2- 1 .8330 .2250 .7500 1.0 0.3333  
O 2- 2 .4550 .2750 .2500 1.0 0.3333  
O 2- 3 .8330 .4670 .2500 1.0 0.3333  
O 2- 4 1.2110 .5330 1.7500 1.0 0.3333  
O 2- 5 .3330 .2750 1.2500 1.0 0.3333  
O 2- 6 .7110 .4670 1.2500 1.0 0.6667  
O 2- 7 .3330 .5330 .7500 1.0 0.3333  
O 2- 8 .7110 .7250 .7500 1.0 0.3333  
O 2- 9 1.2110 .7750 1.2500 1.0 0.3333  
O 2- 10 .8330 .7250 1.7500 1.0 0.6667  
O 2- 11 .8330 .9670 1.2500 1.0 0.3333  
O 2- 12 .3330 1.0330 1.7500 1.0 0.3333  
O 2- 13 .7110 1.2250 1.7500 1.0 0.3333  
O 2- 14 1.2110 1.2750 2.2500 1.0 0.3333  
O 2- 15 .8330 1.2250 2.7500 1.0 0.3333  
O 2- 16 1.2110 1.0330 2.7500 1.0 0.3333  
O 2- 17 .7110 .9670 2.2500 1.0 0.6667  
O 2- 18 .3330 .7750 2.2500 1.0 0.3333  
O 2- 19 .4550 .7750 1.2500 1.0 0.3333  
O 2- 20 1.0890 .5330 .7500 1.0 0.3333  
O 2- 21 1.0890 1.0330 1.7500 1.0 0.3333

#### STACKING

explicit

random 500

{Header for stacking description}

{Statistical ensemble}

{Infinite number of layers}

#### TRANSITIONS

{Transitions from layer 1}

0.785 0.0 0.0 1.0

0.135 0.0 -0.242 0.5

{Header for stacking transition data}

{layer 1 to layer 1}

{layer 1 to layer 2}

0.04	0.0	0.0	1.0	{layer 1 to layer 3}
0.04	0.0	-0.242	0.5	{layer 1 to layer 4}

{Transitions from layer 2}

0.785	0.0	0.0	1.0	{layer 2 to layer 1}
0.135	0.0	-0.242	0.5	{layer 2 to layer 2}
0.04	0.0	0.0	1.0	{layer 2 to layer 3}
0.04	0.0	-0.242	0.5	{layer 2 to layer 4}

{Transitions from layer 3}

0.785	0.0	0.0	1.0	{layer 3 to layer 1}
0.135	0.0	-0.242	0.5	{layer 3 to layer 2}
0.04	0.0	0.0	1.0	{layer 3 to layer 3}
0.04	0.0	-0.242	0.5	{layer 3 to layer 4}

{Transitions from layer 4}

0.785	0.0	0.0	1.0	{layer 4 to layer 1}
0.135	0.0	-0.242	0.5	{layer 4 to layer 2}
0.04	0.0	0.0	1.0	{layer 4 to layer 3}
0.04	0.0	-0.242	0.5	{layer 4 to layer 4}